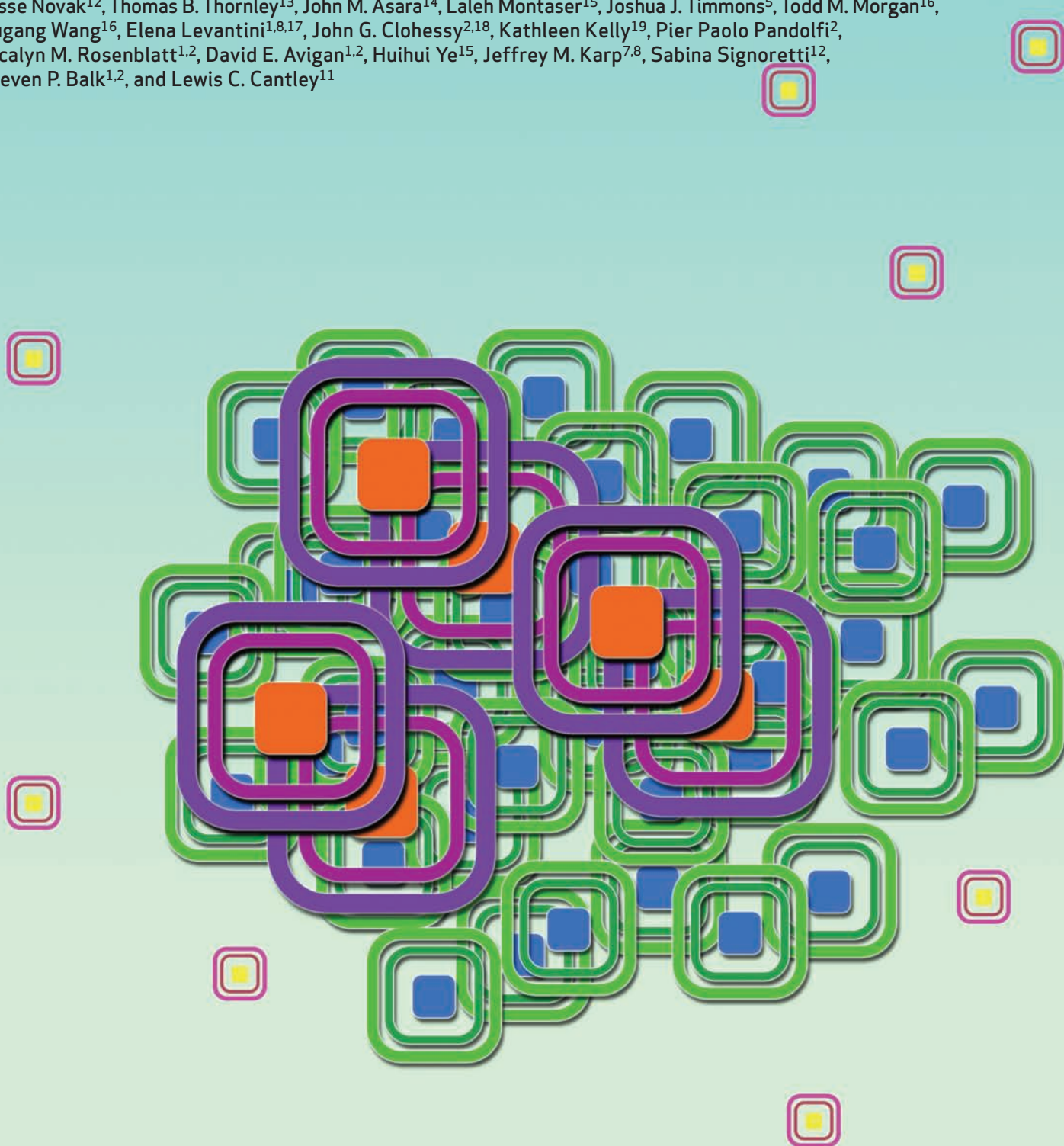


RESEARCH ARTICLE

Cabozantinib Eradicates Advanced Murine Prostate Cancer by Activating Antitumor Innate Immunity

Akash Patnaik^{1,2,3,4}, Kenneth D. Swanson⁵, Eva Csizmadia⁶, Aniruddh Solanki^{7,8}, Natalie Landon-Brace^{7,8}, Marina P. Gehring^{5,9}, Katja Helenius¹⁰, Brian M. Olson^{3,4}, Athalia R. Pyzer¹, Lily C. Wang¹¹, Olivier Elemento¹¹, Jesse Novak¹², Thomas B. Thornley¹³, John M. Asara¹⁴, Laleh Montaser¹⁵, Joshua J. Timmons⁵, Todd M. Morgan¹⁶, Yugang Wang¹⁶, Elena Levantini^{1,8,17}, John G. Clohessy^{2,18}, Kathleen Kelly¹⁹, Pier Paolo Pandolfi², Jacalyn M. Rosenblatt^{1,2}, David E. Avigan^{1,2}, Huihui Ye¹⁵, Jeffrey M. Karp^{7,8}, Sabina Signoretti^{1,2}, Steven P. Balk^{1,2}, and Lewis C. Cantley¹¹



ABSTRACT

Several kinase inhibitors that target aberrant signaling pathways in tumor cells have been deployed in cancer therapy. However, their impact on the tumor immune microenvironment remains poorly understood. The tyrosine kinase inhibitor cabozantinib showed striking responses in cancer clinical trial patients across several malignancies. Here, we show that cabozantinib rapidly eradicates invasive, poorly differentiated PTEN/p53-deficient murine prostate cancer. This was associated with enhanced release of neutrophil chemotactic factors from tumor cells, including CXCL12 and HMGB1, resulting in robust infiltration of neutrophils into the tumor. Critically, cabozantinib-induced tumor clearance in mice was abolished by antibody-mediated granulocyte depletion or HMGB1 neutralization or blockade of neutrophil chemotaxis with the CXCR4 inhibitor plerixafor. Collectively, these data demonstrate that cabozantinib triggers a neutrophil-mediated anticancer innate immune response, resulting in tumor clearance.

SIGNIFICANCE: This study is the first to demonstrate that a tyrosine kinase inhibitor can activate neutrophil-mediated antitumor innate immunity, resulting in invasive cancer clearance. *Cancer Discov*; 7(7); 750–65. ©2017 AACR.

INTRODUCTION

Malignant cells and stromal cells cooperate to create an immunosuppressive microenvironment that protects developing tumors from immune eradication (1). Paul Ehrlich first postulated a pathologically important relationship between the immune system and cancer, suggesting that a breakdown in normal antitumor immune surveillance occurs as a part of tumor evolution (2). The growing tumor subverts the immune system's normal wound-healing mechanisms, exploiting them for tumor protection, maintenance, and progression (3). Attempts to perturb this collaborative relationship between the tumor and its immune stroma date back approximately 125 years to William Coley, who injected bacterial lysates into the tumor bed in an attempt to stimulate tumor rejection (4). There has been a resurgent interest in cancer immunotherapy, partly based on the profound and durable clinical responses to T lymphocyte checkpoint control antibodies against CTLA-4 and PD-1/PD-L1. However, there are still subsets of patients across all malignancies that fail to respond to these therapies. Although there have been

several approaches developed to activate the adaptive arm of the immune system for cancer elimination, strategies to activate antitumor innate immunity have remained elusive.

Cabozantinib (also known as XL-184) is a promiscuous receptor tyrosine kinase (RTK) inhibitor with potent activity against c-MET, VEGFR2, RET, KIT, AXL, and FLT3, all of which have been implicated in tumor growth and survival (5). Cabozantinib has been approved by the FDA for the treatment of medullary thyroid cancer (MTC), a RET-driven malignancy (6). In a phase II randomized discontinuation trial in patients with castrate-resistant prostate cancer (CRPC), 72% of patients exhibited regression in soft-tissue lesions, whereas 68% of patients had improvement in technetium-99m bone scan response, including complete resolution in 12%. This dramatic bone scan response is unprecedented in CRPC with bone metastases treated with current standard-of-care therapies. The trial exhibited a median progression-free survival (PFS) of 23.9 versus 5.9 weeks for the cabozantinib- and placebo-treated cohorts, respectively, with significant reductions in bone turnover markers and bone pain with cabozantinib treatment (7).

¹Division of Hematology/Oncology, Department of Medicine, Beth Israel Deaconess Medical Center, Dana Farber/Harvard Cancer Center, Harvard Medical School, Boston, Massachusetts. ²Beth Israel Deaconess Cancer Center, Department of Medicine, Beth Israel Deaconess Medical Center, Harvard Medical School, Boston, Massachusetts. ³Section of Hematology/Oncology, Department of Medicine, The University of Chicago, Chicago, Illinois. ⁴The University of Chicago Comprehensive Cancer Center, Chicago, Illinois. ⁵Department of Neurology, Beth Israel Deaconess Medical Center, Harvard Medical School, Boston, Massachusetts. ⁶Division of Gastroenterology, Department of Medicine, Beth Israel Deaconess Medical Center, Boston, Massachusetts. ⁷Department of Medicine, Brigham and Women's Hospital, Harvard Medical School, Boston, Massachusetts. ⁸Harvard Stem Cell Institute, Boston, Massachusetts. ⁹Laboratório de Farmacologia Aplicada, PUCRS, Porto Alegre, Brazil. ¹⁰Koch Institute for Integrative Cancer Research, Massachusetts Institute of Technology, Cambridge, Massachusetts. ¹¹Meyer Cancer Center, Weill Cornell Medical College, New York, New York. ¹²Department of Pathology, Brigham and Women's Hospital, Harvard Medical School, Boston, Massachusetts. ¹³Transplant Institute and Immunology Program, Beth Israel Deaconess Medical Center, Harvard Medical School, Boston, Massachusetts. ¹⁴Division of Signal Transduction, Beth

Israel Deaconess Medical Center, Harvard Medical School, Boston, Massachusetts. ¹⁵Department of Pathology, Beth Israel Deaconess Medical Center, Harvard Medical School, Boston, Massachusetts. ¹⁶Department of Urology, University of Michigan, Ann Arbor, Michigan. ¹⁷Institute of Biomedical Technologies, National Research Council (CNR), Pisa, Italy. ¹⁸Preclinical Murine Pharmacogenetics Facility, Beth Israel Deaconess Medical Center, Harvard Medical School, Boston, Massachusetts. ¹⁹Laboratory of Genitourinary Cancer Pathogenesis, National Cancer Institute, Bethesda, Maryland.

Note: Supplementary data for this article are available at *Cancer Discovery* Online (<http://cancerdiscovery.aacrjournals.org/>).

M.P. Gehring, K. Helenius, B.M. Olson, and A.R. Pyzer contributed equally to this article.

Corresponding Author: Akash Patnaik, The University of Chicago, Knapp Center for Biomedical Discovery, Room 7152, 900 East 57th Street, Chicago, IL 60637. Phone: 773-834-3519; Fax: 773-834-0778; E-mail: apatnaik@uchicago.edu

doi: 10.1158/2159-8290.CD-16-0778

©2017 American Association for Cancer Research.

RESEARCH ARTICLE

Despite promising phase II clinical trial results, a recent phase III trial of cabozantinib in patients with heavily pretreated metastatic CRPC (COMET-1) failed to demonstrate a statistically significant increase in overall survival (OS) with cabozantinib versus prednisone alone. Consistent with the previous phase II results, median radiographic PFS (HR, 0.48; 95% CI, 0.40–0.57; stratified log-rank $P < 0.001$) was 5.6 versus 2.8 months for the cabozantinib versus prednisone arms, respectively (8). Moreover, a randomized phase III trial (METEOR) of cabozantinib versus everolimus in VEGFR inhibitor-resistant renal cell cancer (RCC) showed a 42% decrease in disease progression (9, 10). Therefore, a deeper understanding of cabozantinib's antitumor mechanism is critical for biomarker-based stratification of patients most likely to respond to the drug.

Loss of PTEN and p53 function are frequent genetic events in human CRPC (11, 12). Mice with probasin Cre-driven conditional prostate-specific knockout of *Pten* and *Trp53* (*Pb-Cre; Pten^{f/f}Trp53^{f/f}*) develop invasive CRPC (13) as early as 9 weeks and locally aggressive tumors by 3 months of age, that are invariably lethal to the host by 7 months of age (14). Here, we show that cabozantinib eradicated poorly differentiated invasive adenocarcinoma in these mice within 48 hours, with concomitant infiltration of neutrophils into the tumor bed. Strikingly, neutrophil depletion or chemotaxis blockade with either an HMGB1-neutralizing monoclonal antibody or the CXCR4 inhibitor plerixafor reversed the tumor clearance elicited by cabozantinib. These data provide strong evidence that cabozantinib elicits a neutrophil-mediated anticancer innate immune response that results in tumor eradication.

RESULTS

Cabozantinib Eradicates Murine Prostate Cancer via a c-MET-Independent Immune Mechanism

Cabozantinib was developed as a c-MET/VEGFR2 inhibitor (5). Previous studies have shown *Met* amplification in 67% of prostate tumors from *Pb-Cre; Pten^{f/f}Trp53^{f/f}* mice and in approximately 30% of metastatic PTEN and p53-deficient human prostate cancer specimens (15). As a first step toward evaluating whether the antitumor mechanism of cabozantinib is c-MET dependent, we tested its effect on aggressive prostate cancers that develop in 5- to 6-month-old *Pb-Cre; Pten^{f/f}Trp53^{f/f}* mice. The mice were treated with vehicle, cabozantinib, or PF-04217903 (c-MET-specific inhibitor) after the solid tumor had reached a long-axis diameter of at least 5 mm by ultrasound and MRI analysis. Cabozantinib-treated mice showed an approximately 70% reduction in tumor volume (Fig. 1A and B), which was accompanied by decreased FDG-PET signal (Supplementary Fig. S1). Strikingly, histopathology revealed a near-complete clearance of the poorly differentiated, invasive prostate carcinoma in 4 days, which was sustained over 3 weeks of cabozantinib treatment (Fig. 1C). In contrast, PF-04217903 failed to inhibit tumor growth (Fig. 1A and B) over 3 weeks of treatment, despite similar inhibition of intratumoral phospho-MET with both cabozantinib and PF-04217903 (Supplementary Fig. S2A). Prostate tumors from PF-04217903-treated mice exhibited a persistence of poorly differentiated, invasive prostate carcinoma after 3 weeks of treatment (Fig. 1C, top

middle). These data demonstrated that c-MET inhibition alone was insufficient to explain cabozantinib's antitumor mechanism of action.

Cabozantinib Treatment Results in Rapid Neutrophil Infiltration into the Tumor Bed

In light of this profound antitumor response to cabozantinib in 4 days, we performed detailed histopathologic evaluation of prostate tumors from treated mice over the initial 72-hour time period. This analysis revealed a near-complete eradication of poorly differentiated invasive adenocarcinoma within 48 to 72 hours of treatment (Fig. 2A, hematoxylin and eosin panel). This was accompanied by increased perivascular ICAM1 staining and hypersegmented (see the inset in Fig. 2A), Ly6G⁺, myeloperoxidase⁺ (MPO⁺) neutrophil infiltration into the tumor within 24 to 48 hours of treatment (Fig. 2A). Flow cytometry also showed an increase in CD11b⁺GR1⁺ tumor-infiltrating immune cells following 72 hours of cabozantinib treatment (Fig. 2B). Further immune surface marker analysis demonstrated that these cells were Ly6G^{hi}Ly6C^{lo}, consistent with a granulocytic (and not monocytic) predominance of tumor-infiltrating immune cells following cabozantinib treatment (Supplementary Fig. S2B).

Cabozantinib Induces *In Vivo* Tumor Cell Death via CXCL12-HMGB1-CXCR4-Dependent Neutrophil Recruitment

The near-complete tumor clearance elicited by cabozantinib was preceded by a significant increase in caspase-3 staining *in vivo* (Fig. 3A). If cabozantinib exerts its antitumor effects via a cell-autonomous mechanism, then treatment of murine PTEN/p53-deficient tumor-derived prostate cancer cells *in vitro* would be expected to result in a similar dramatic induction of apoptosis. To determine the physiologically relevant cabozantinib dose for *in vitro* apoptosis experiments, we performed mass spectrometry analysis of prostate tumor-extracted metabolites from cabozantinib-treated mice. This revealed a steady-state intratumoral concentration of approximately 10 μmol/L within 72 hours after treatment (Supplementary Fig. S3A), which is in a similar range to the steady-state serum concentration observed in cabozantinib-treated patients (16). RTK profiling of the human androgen-independent prostate cancer cell line PC3 revealed that cabozantinib at 10 μmol/L concentration inhibits multiple RTKs (Supplementary Fig. S3B). We therefore tested three murine PTEN/p53 deficient prostate tumor cell lines, SC1, AC1, and AC3, for apoptosis induction *in vitro* at physiologic concentrations. In contrast to the rapid induction of caspase-3 staining by cabozantinib *in vivo* (Fig. 3A), we detected only modest apoptosis *in vitro* at similar time points, even at a high concentration of 30 μmol/L (Fig. 3B). These results suggest that the direct induction of apoptosis is not the dominant cell death mechanism observed *in vivo* following cabozantinib treatment.

To further explore the mechanism of cabozantinib-mediated acute tumor clearance *in vivo*, we performed transcriptional profiling and gene set enrichment analysis of prostate tumors recovered from *Pb-Cre; Pten^{f/f}Trp53^{f/f}* mice following 48 hours of cabozantinib treatment versus control untreated tumors. This analysis revealed a statistically significant upregulation

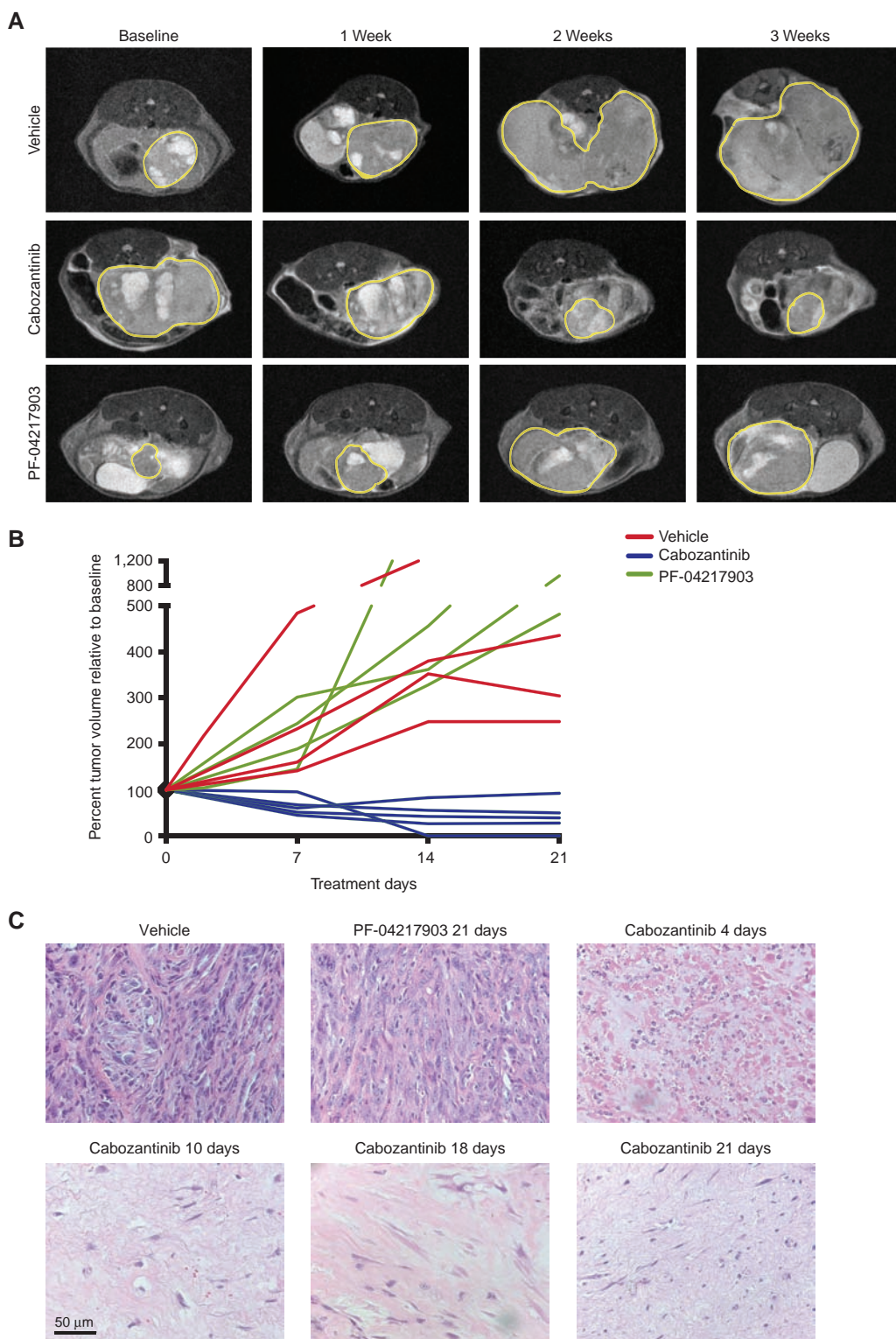


Figure 1. Cabozantinib causes tumor regression and near-complete clearance of invasive poorly differentiated murine prostate cancer. **A**, Representative MRI images showing the relative impact of vehicle (top), cabozantinib (middle), and the c-MET inhibitor PF-04217903 (bottom), on regression of established murine PTEN/p53-deficient prostate tumors. Mice were treated with the indicated drugs at the following concentrations: vehicle control, cabozantinib (100 mg/kg), and PF-04217903 (50 mg/kg). The yellow borders mark solid tumor boundaries during the 3-week course of treatment. **B**, Volumetric analysis showed significant tumor regression in mice treated with cabozantinib, but not vehicle or PF-04217903 treatment. **C**, Hematoxylin and eosin (H&E) staining of tumors from cabozantinib-treated mice revealed near-complete eradication of poorly differentiated prostate tumors at 4, 10, 18, and 21 days of treatment, not observed with vehicle- or PF-04217903-treated mice ($n = 4$ mice per treatment arm/time point).

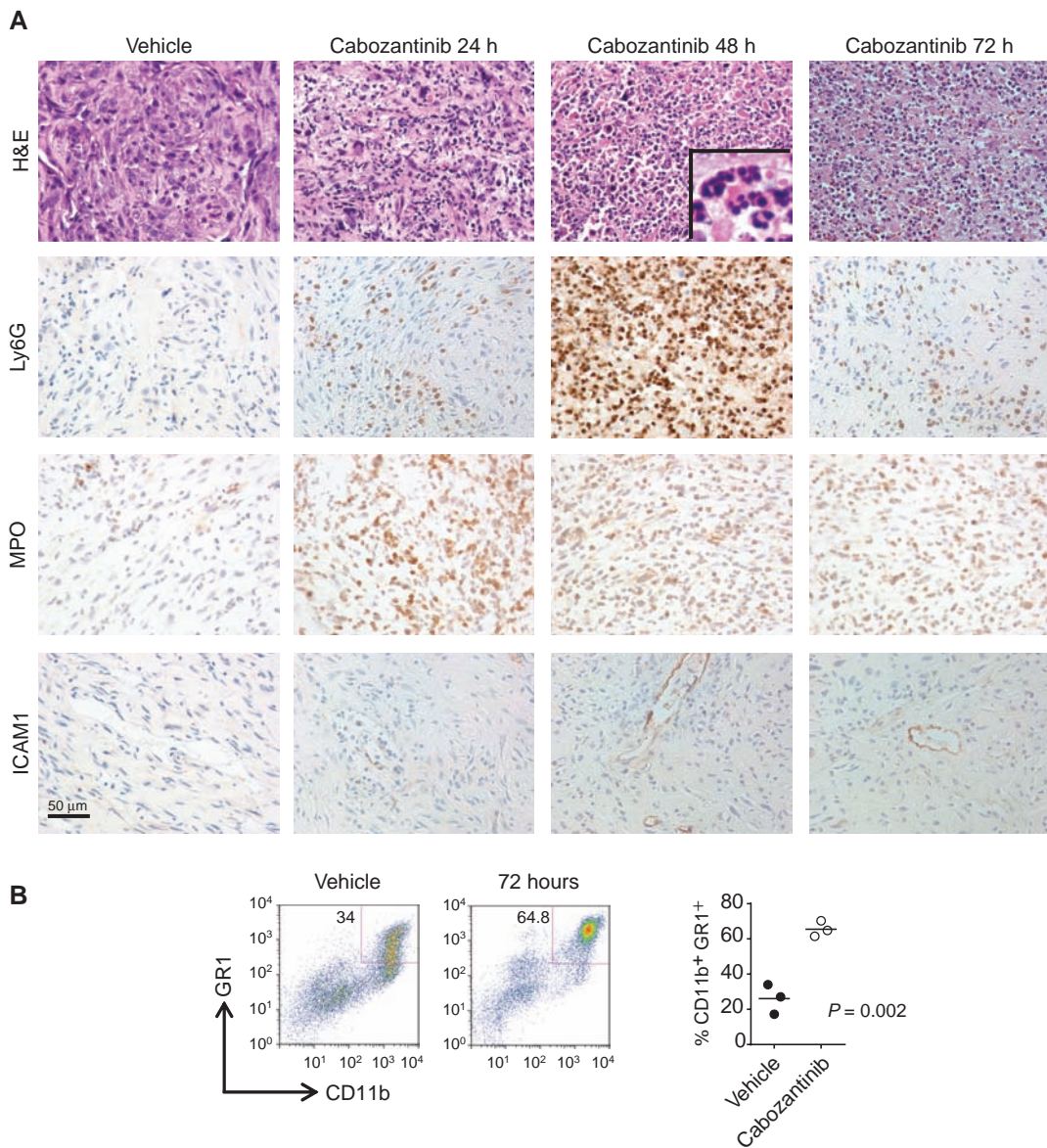


Figure 2. Cabozantinib induces extensive infiltration of neutrophils into the tumor bed and near-complete clearance of invasive poorly differentiated murine prostate cancer within 48 to 72 hours of drug treatment. **A**, H&E, Ly6G, MPO, and ICAM1 staining of established prostate tumors harvested from *Pb-Cre; Pten^{f/f}; Trp53^{f/f}* mice treated with vehicle, 24, 48, and 72 hours of cabozantinib (100 mg/kg) treatment, respectively. Mice were treated with vehicle or cabozantinib for the indicated times, and tumor tissues were stained with either H&E or the indicated antibodies by IHC. These data show an increase in Ly6G-positive and MPO-positive neutrophils, and an increase in ICAM1-positive endothelium within 48 hours of cabozantinib treatment. **B**, Flow cytometry analysis of dissociated tumor showed a similar increase in CD11b⁺GR1⁺ tumor-infiltrating neutrophils with cabozantinib treatment.

of immune response transcripts following cabozantinib treatment *in vivo* (Fig. 4A). Subsequent qPCR-based RNA profiling of cabozantinib-treated tumors revealed a spike in gene expression of the chemokine CXCL12 and its receptor CXCR4 within the tumor microenvironment following 24 hours of cabozantinib treatment (Fig. 4B). CXCR4 is implicated in lymphocyte (17) and neutrophil chemotaxis (18) from the periphery. CXCR4 can engage CXCL12 as a homodimer or a 2:1 heterocomplex of CXCL12 and HMGB1, the latter serving as a danger signal during immunogenic cell death (19, 20).

The tumor microenvironment is a complex admixture of transformed tumor cells and nontransformed stromal cells,

including a diverse population of immune cells (21). Tumor cells can secrete a number of chemokines that cross-talk with different stromal cells within the microenvironment and alter innate and adaptive immune function (21, 22). To determine the predominant cell type within the tumor responsible for cabozantinib-induced production of CXCL12, we performed RNA *in situ* hybridization (RISH) for CXCL12 followed by PTEN IHC on prostate tumors from mice treated with vehicle or 24 hours of cabozantinib. Consistent with our qPCR results, we observed an increase in intratumoral CXCL12 staining by RISH following cabozantinib treatment specifically in PTEN-deficient cells within the microenvironment (Fig. 4C;

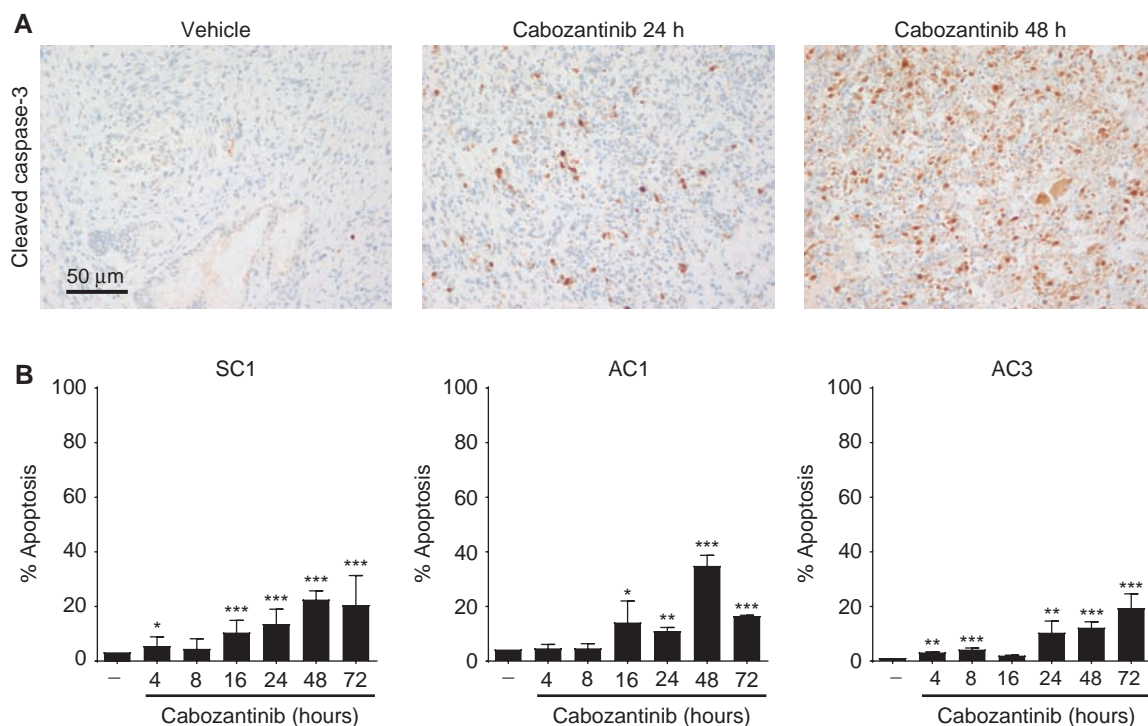


Figure 3. Cabozantinib causes significant tumor cell elimination *in vivo*, but modest apoptosis induction *in vitro*. **A**, Cabozantinib acutely increased caspase-3 staining within 24 to 48 hours of treatment in established murine PTEN/p53-deficient prostate tumors. Mice were treated with cabozantinib for the indicated times, and prostate tumor tissues were stained with caspase-3 antibody by IHC. Images show representative sections from $n = 3$ mice per time point. **B**, PTEN/p53-deficient prostate tumor-derived cell lines treated with cabozantinib showed only modest cell death. SC1, AC1, and AC3 cells were treated with 30 μ mol/L cabozantinib for the indicated times, followed by apoptosis analysis with Annexin V staining ($n = 3$ experiments). *, $P < 0.05$; **, $P < 0.01$; ***, $P < 0.001$.

Supplementary Fig. S4A), suggesting that the increase in CXCL12 expression was predominantly occurring in the tumor cells (Fig. 4C, bottom). These *in vivo* findings were supported by analysis of PTEN/p53-deficient tumor-derived SC1 cells treated with cabozantinib for 24 hours *ex vivo*, which revealed increased CXCL12 release into the supernatant by ELISA (Fig. 4D). These data demonstrate that cabozantinib treatment drives CXCL12 expression within the cancer cells in the tumor microenvironment.

Classically defined apoptosis is immunosuppressive, due to translocation of phosphatidylserine to the cell surface that interacts with the TIM4 immune inhibitory receptor on myeloid cells (23). In contrast, immunogenic cell death (ICD) represents an evolved program that triggers a productive immune response against the dying cells. During ICD, the endoplasmic reticulum chaperone calreticulin is exposed on the cell surface and serves as an “eat me” signal to promote recognition and phagocytosis by innate immune cells. In addition, ATP and HMGB1 are actively secreted and serve to attract and activate granulocytes and other infiltrating immune cells (23). These three events are collectively considered hallmarks of ICD (24). To evaluate the possibility that cabozantinib evokes an ICD-like response via HMGB1 release and heterocomplex formation with CXCL12 to engage the CXCR4 receptor (19), we asked whether *ex vivo* cabozantinib treatment of PTEN/p53-deficient tumor-derived SC1 cells resulted in the release of HMGB1. ELISA analysis revealed

an increase in HMGB1 release into the supernatant following *ex vivo* cabozantinib treatment of SC1 cells for 32 hours (Fig. 4E), with a similar response to that observed with the known ICD inducer doxorubicin (24). Consistent with increased extracellular release of HMGB1, we observed a decrease in cytosolic levels of HMGB1 in doxorubicin- and cabozantinib-treated SC1 cells, indicative of cellular depletion (Fig. 4F). In contrast, *PTEN* wild-type, *TP53*-mutant human prostate cancer cells VCaP, DU145, and 22Rv1 did not exhibit increased HMGB1 release following cabozantinib treatment (Supplementary Fig. S4B).

Further characterization of the acute immunologic response in PTEN/p53-deficient prostate tumors from mice treated with cabozantinib revealed an increase in intratumoral CD86 expression by IHC and qRT-PCR (Supplementary Fig. S5A and S5B) and an increase in CD11b⁺CD86⁺ cells by flow cytometry (Supplementary Fig. S5C), demonstrating maturation and activation of myeloid antigen-presenting cells. Taken together, these data demonstrate that cabozantinib triggers release of CXCL12 and HMGB1 from dying PTEN/p53-deficient tumor cells, resulting in activation of an antitumor immune response.

Neutrophils Are Required for Cabozantinib-Induced Tumor Clearance

To determine whether cabozantinib-induced tumor clearance occurs via increased infiltration of T cells and/or natural

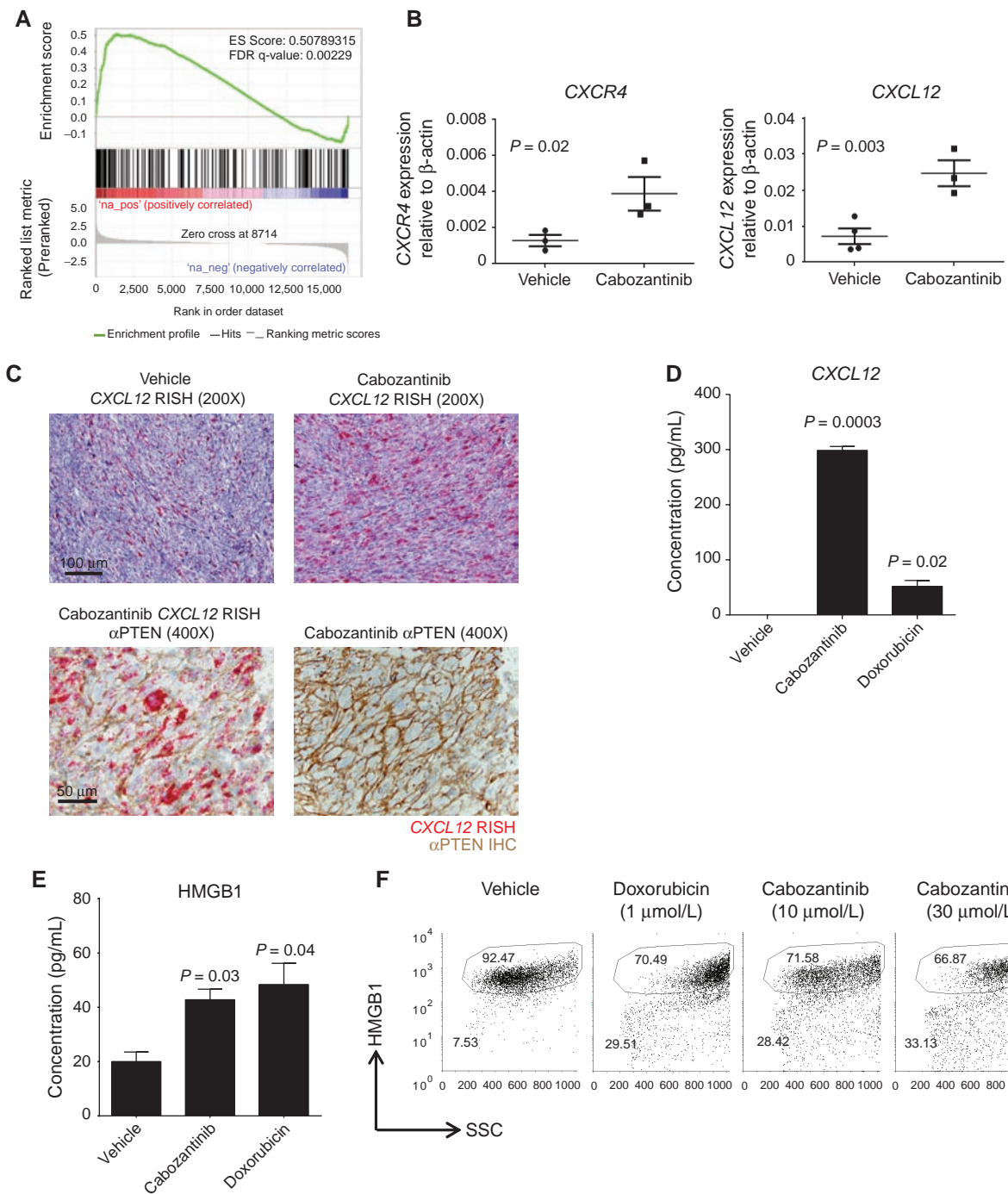


Figure 4. Cabozantinib treatment causes significant upregulation of CXCL12 and HMGB1 levels within the tumor microenvironment. **A**, *Pb-Cre; Pten^{f/f}/Trp53^{f/f}* mice with established prostate tumors were treated with cabozantinib at 100 mg/kg daily for 48 hours followed by tumor RNA extraction. Gene set enrichment analysis revealed a highly increased expression of immune response related gene sets. **B**, Mice were treated with cabozantinib as above for 24 hours followed by tumor RNA extraction. Quantitative RT-PCR analysis was performed for several immune response genes and showed a statistically significant upregulation of CXCL12 and CXCR4 gene expression with cabozantinib treatment ($n = 3$ mice per time point). **C**, CXCL12 RISH of tumors from mice acutely treated with cabozantinib for 24 hours revealed increased intratumoral CXCL12 expression (top). Combined CXCL12 RISH and PTEN IHC from these tumors showing that the PTEN-deficient prostate cancer cells within the tumor microenvironment are producing CXCL12 (bottom) following cabozantinib treatment. Representative staining from $n = 3$ mice per condition. Increased release of CXCL12 (**D**) and HMGB1 (**E**) following *in vitro* treatment of murine tumor-derived prostate cancer cells with cabozantinib. SC1 cells were treated with vehicle, cabozantinib (10 μ mol/L), or doxorubicin (1 μ mol/L) for 24 hours. Supernatants were analyzed for CXCL12 and HMGB1 by ELISA. **F**, SC1 cells were treated with vehicle, cabozantinib (10 μ mol/L), or doxorubicin (1 μ mol/L) for 28 hours and subjected to FACS analysis, demonstrating cabozantinib-induced HMGB1 depletion ($n = 3$ experiments for **D-F**).

killer (NK) cells into the tumor bed, we performed qRT-PCR on prostate tumors from mice treated with cabozantinib for 24 hours. Interestingly, we observed no increase in gene expression of *CD3*, *CD4*, *CD8* (T-cell markers), or *NKG2D* (NK and activated CD8 T-cell marker) gene expression following cabozantinib treatment (Supplementary Fig. S6A). If intratumoral resident NK and T cells play a dominant role in the antitumor immune response, then removal of these cell types, singly and/or in combination, should attenuate the effects of cabozantinib on tumor clearance. To test this hypothesis, *Pb-Cre; Pten^{f/f}Trp53^{f/f}* mice were pretreated with antibodies directed against CD4/CD8 and anti-sialo GM1 to deplete conventional T-cell subsets (Supplementary Fig. S6B) and NK cells (Supplementary Fig. S6C), respectively, followed by coadministration of cabozantinib. We found that neither the CD4/CD8 nor NK-depleting antibodies, singly or in combination, attenuated the tumor clearance elicited by cabozantinib (Supplementary Fig. S6D), suggesting that its antitumor immunologic mechanism is independent of both conventional T and NK cells.

The infiltration of neutrophils into the tumor bed within 48 hours of cabozantinib treatment suggested that neutrophil effector function might play a role in tumor clearance (25–29). If the tumor clearance elicited by cabozantinib is mediated by infiltrating neutrophils, then this response should be abolished by concomitant granulocyte depletion or chemotaxis blockade with dexamethasone (30, 31) or the CXCR4 inhibitor plerixafor (32, 33) or HMGB1 neutralization (34). On the other hand, if cabozantinib's antitumor effects are mediated via intratumoral suppression of tumor-promoting CD11b⁺/GR1⁺ granulocytic myeloid-derived suppressor cells (MDSC), then cabozantinib-induced tumor clearance should be unaffected by concomitant Ly6G⁺ granulocyte depletion or blockade of granulocyte chemotaxis. To test these possibilities, tumor-bearing *Pb-Cre; Pten^{f/f}Trp53^{f/f}* mice were pretreated with anti-Ly6G-depleting antibody (1A8) or the CXCR4 inhibitor plerixafor, followed by concomitant 1A8 or plerixafor, respectively, and cabozantinib. In addition, we also evaluated the impact of HMGB1 neutralization (3E8) on the tumor clearance elicited by cabozantinib. Combinatorial treatments with 1A8 antibody/cabozantinib treatment, plerixafor/cabozantinib, and 3E8/cabozantinib treatment all resulted in a complete loss of expression of the granulocytic marker Ly6G and neutrophil-specific marker MPO within the tumor bed, relative to cabozantinib alone, demonstrating an absence of tumor-infiltrating neutrophils. Critically, the increased caspase-3 staining and near-complete tumor eradication observed with cabozantinib alone was abolished with 1A8 antibody/cabozantinib, plerixafor/cabozantinib, and 3E8/cabozantinib combination treatment (Fig. 5A). This demonstrates a necessary role for tumor-infiltrating neutrophils in cabozantinib-induced tumor clearance. Moreover, there was a direct correlation between the magnitude of neutrophil infiltration (Fig. 5B) and tumor caspase-3 staining across different treatment groups (Fig. 5C). Long-term treatment of mice with plerixafor/cabozantinib and 3E8/cabozantinib treatment interfered with cabozantinib's ability to induce tumor regression (Supplementary Fig. S7A and S7B), with histopathologic persistence of tumor at the end of 2 weeks of cotreatment (Supplementary Fig. S7C).

In addition, this neutrophil-mediated tumor clearance elicited by cabozantinib was also attenuated by dexamethasone (Supplementary Fig. S8), which is known to inhibit neutrophil chemotaxis (30). Taken together, these data demonstrate that cabozantinib eradicates murine invasive PTEN/p53-deficient prostate cancer via activation of an HMGB1- and CXCR4-dependent, neutrophil-mediated antitumor innate immune response.

If soluble tumor-secreted factors are responsible for neutrophil chemotaxis and activation within PTEN/p53-deficient tumors *in vivo*, then *ex vivo* treatment of tumor cells with cabozantinib should enhance neutrophil effector function. To test this hypothesis, we subjected human neutrophils to chemotaxis and activation in transwell migration and nitric oxide (NO) release assays, respectively. Consistent with our *in vivo* findings, we found that cabozantinib treatment of PC3 human prostate cancer cells in the lower chambers of transwells resulted in a >3-fold increase in neutrophil migration from the upper chambers (Fig. 6A) and a 20% increase in neutrophils with NO staining in cocultured neutrophils (Fig. 6B), respectively. In the absence of tumor cells, cabozantinib treatment did not enhance neutrophil migration or increase NO staining, suggesting that the increased migration/activation occurs via tumor-secreted factors, and not via a direct effect of cabozantinib on neutrophils *per se* (Fig. 6A–C). Furthermore, the enhancement of neutrophil chemotaxis elicited by cabozantinib was completely abrogated by concomitant HMGB1 depletion (3E8) antibody (Fig. 6C). Taken together, these data confirm the critical role of cabozantinib-mediated HMGB1 release from tumor cells, resulting in enhanced neutrophil chemotaxis and activation. This reprogramming of the tumor inflammatory/immune chemokine network within the tumor microenvironment triggers a robust neutrophil infiltration and invasive cancer eradication (Fig. 6D).

DISCUSSION

There is an emerging body of evidence that highlights the impact of kinase inhibitors on the tumor immune microenvironment. For example, BRAF inhibitors approved for the treatment of V600E-mutant metastatic melanoma decrease the release of immunosuppressive cytokines, resulting in decreased MDSCs and regulatory T cells (Treg). This reprogramming of the immune microenvironment results in an increase in both MHC class I-mediated antigen presentation and T-cell infiltration (35, 36), thus unleashing host-adaptive anticancer immunity. Furthermore, recent studies have shown that HLA class I downregulation is associated with enhanced NK-cell killing of melanoma cells with acquired drug resistance to BRAF inhibitors (37). In contrast, the MEK inhibitor trametinib alone or in combination with the BRAF inhibitor dabrafenib suppressed T-lymphocyte proliferation, cytokine production, and antigen-specific expansion. Monocyte-derived dendritic cell cross-presentation was also suppressed following combined inhibition of MEK and BRAF (38). Moreover, the MEK inhibitor PD0325901 induced the downregulation of NK-activating receptors, thus inhibiting NK-cell function (39), suggesting that MEK inhibitors may have a detrimental effect on anticancer immune activation.

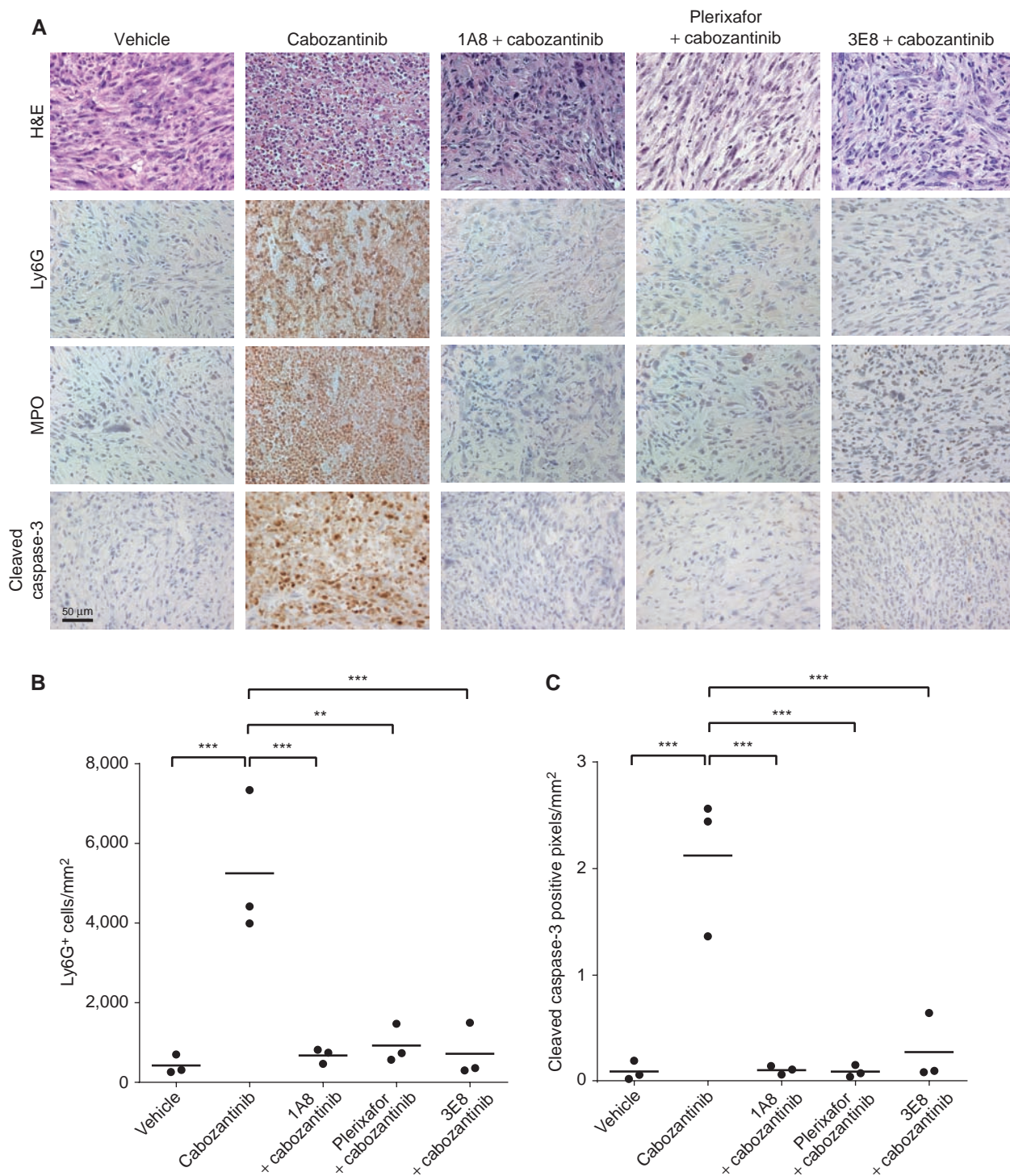


Figure 5. Depletion of neutrophils or blockade of neutrophil chemotaxis/infiltration abolishes cabozantinib-induced tumor clearance. **A**, *Pten*^{f1/f1}*Trp53*^{f1/f1} mice were treated as indicated (from left to right): untreated control; vehicle pretreatment for 3 days, followed by cabozantinib treatment for an additional 3 days; 1A8 (Ly6G antibody) pretreatment for 3 days, followed by concomitant 1A8/cabozantinib treatment for an additional 3 days; AMD3100 (CXCR4 inhibitor) pretreatment via osmotic pump for 3 days, followed by concomitant AMD3100/cabozantinib treatment for an additional 3 days; concomitant 3E8 (HMGB1 neutralization antibody)/cabozantinib treatment for 3 days (see Methods for details). At the end of treatment, tumor tissues were stained with H&E, Ly6G, MPO, cleaved caspase-3 ($n=3$ mice per treatment group). Ly6G⁺ **(B)** and caspase-3⁺ **(C)** cells were subjected to automated quantification across the entire tumor section on the slide, and reported as cells per unit square area. *, $P < 0.05$; **, $P < 0.01$; ***, $P < 0.001$.

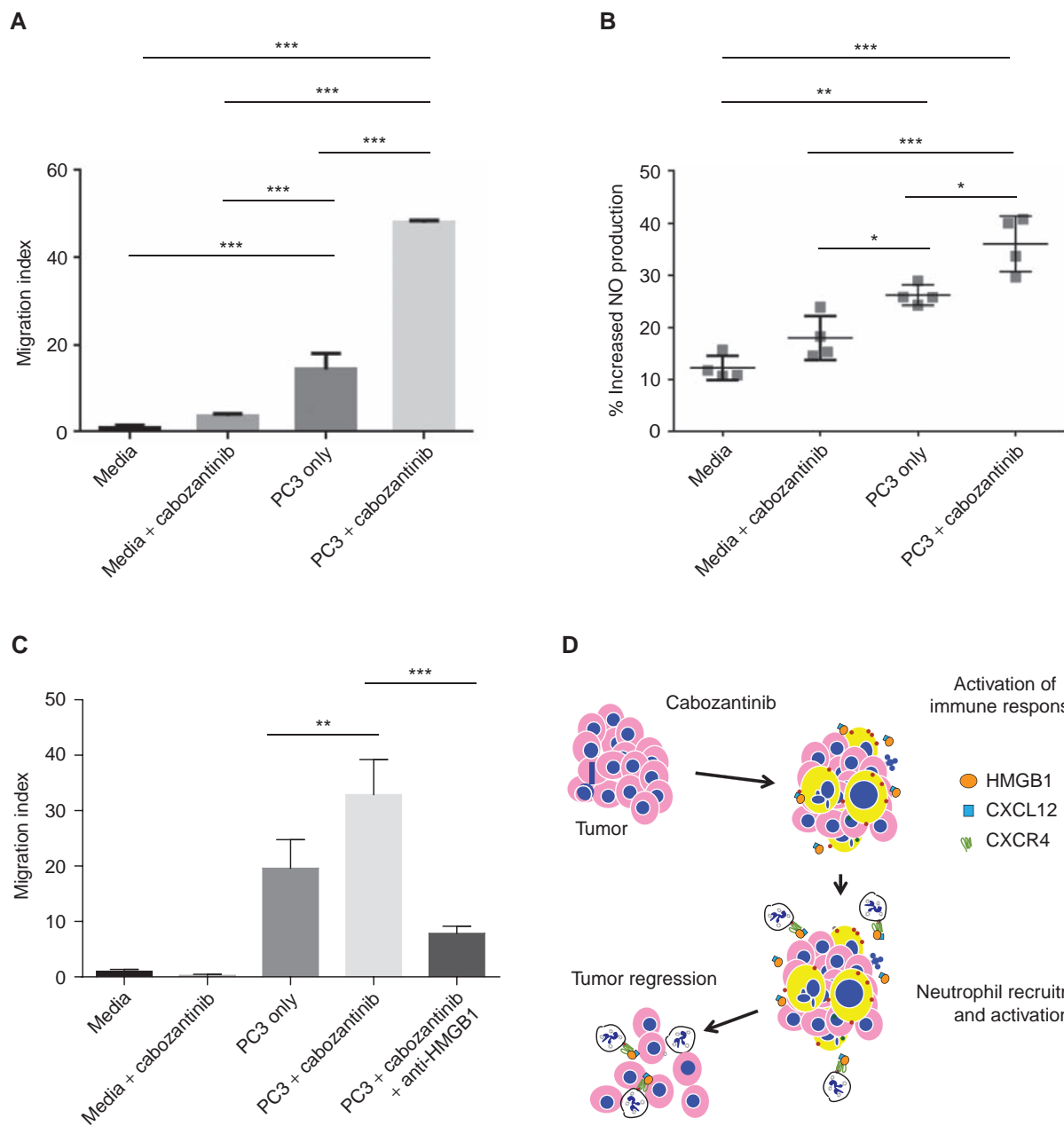


Figure 6. Cabozantinib treatment of human PTEN/p53-deficient prostate cancer cells enhances *ex vivo* HMGB1-dependent neutrophil migration and activation. **A**, PC3 cells were treated with 5 μmol/L cabozantinib for 24 hours, followed by addition of neutrophils in a Transwell migration assay for 4 hours. The neutrophils were obtained from a single patient donor with each condition being performed in 3 separate migration Transwells ($n = 3$ technical repeats). The data are representative of $n = 3$ experiments. The statistical analysis was performed using one-way ANOVA with Sidak's multiple comparison method. **B**, PC3 cells were treated with cabozantinib for 24 hours, and then cocultured with neutrophils for 6 hours, followed by nitric oxide staining and flow cytometry. The results were obtained from 4 separate donors ($n = 4$ biological repeats), with each point (each donor) representing a value that was averaged from 2 to 3 technical repeats. The statistical analysis was performed using one-way ANOVA followed by a Tukey post hoc test. **C**, PC3 cells were treated as described in **A**. For the HMGB1 rescue treatment, anti-HMGB1 clone 3E8 was added to cabozantinib-treated PC3 cells to a final concentration of 50 μg/mL and incubated for one hour at 37°C. The neutrophils were obtained from a single donor, with each condition being performed in 3 separate migration Transwells ($n = 3$ technical repeats). The statistical analysis was performed as in **A**. *, $P < 0.05$; **, $P < 0.01$; ***, $P < 0.001$. **D**, Schematic model for cabozantinib's effects on neutrophil-mediated activation of antitumor innate immunity within the tumor microenvironment, resulting in invasive cancer clearance. The pink cells with blue nuclei represent tumor cells, whereas the yellow enlarged cells with blue nuclei represent tumors undergoing immunogenic cell death following cabozantinib treatment. The white cells represent neutrophils, which are recruited and activated via engagement of CXCR4 with CXCL12/HMGB1 released from tumor cells. This neutrophil recruitment/activation results in tumor cell death.

However, recent *in vivo* studies in a syngeneic BRAF^{V600E}-driven melanoma showed that single-agent BRAF inhibitor (dabrafenib) increased tumor-associated macrophages and Tregs in tumors, which decreased with the addition of the MEK inhibitor (trametinib). Because the combination of BRAF and MEK inhibitors induced PD-L1 expression, the triple combination of dabrafenib, trametinib, and anti-PD-1 therapy resulted in a robust antitumor response, supporting a clinical trial of this combination in patients with BRAF^{V600E}-mutant metastatic melanoma (40).

Therapeutic induction of apoptosis is likely to result in intratumoral immunosuppression and peripheral tolerance toward the transformed cells within the tumor, thus contributing to the development of resistance (24). The majority of kinase inhibitors to date have been exclusively evaluated for their ability to induce apoptosis in a cell-autonomous manner, which may limit their efficacy in the clinic. In this study, we observed that approximately 40% of the total cellular mass of *Pten*^{-/-}; *Trp53*^{-/-} prostate tumors is comprised of CD45⁺ immune cells, the majority of which are CD11b^{hi}GR1^{hi} myeloid suppressor cells. This immune cell population has been previously shown to promote tumor growth via bypass of the senescence response (41). Here, we show that cabozantinib, a promiscuous tyrosine kinase inhibitor, generated a potent neutrophil-mediated antitumor innate immune response that superseded the intratumoral myeloid immunosuppressive milieu, resulting in rapid tumor eradication in a *Pten*^{-/-}; *Trp53*^{-/-}-deficient prostate cancer model.

Neutrophils represent the first step in the generation of an innate immune response during an active infection and are promptly recruited into inflamed tissue via interaction with activated endothelial cells and chemokine gradients (18). Following recruitment/activation, neutrophils are capable of inducing oxidative damage through reactive oxygen species production and protease release (27). Neutrophils are detected in a variety of solid tumors and play multifaceted roles in the tumor microenvironment (28). Neutrophils are functionally capable of acquiring either proinflammatory, antitumor (N1), or protumorigenic (N2) properties, which are regulated by the chemokine context within the tumor microenvironment (26). A recent study in the mammary 4T1 syngeneic model showed that CD11b⁺/Ly6G⁺ neutrophils enhance metastasis of tumor cells via inhibition of NK cell function and promote tumor cell extravasation via secretion of IL1 β and matrix metalloproteinases (42). In contrast, our data are consistent with the model that neutrophils are recruited to the tumor microenvironment via a CXCL12/HMGB1/CXCR4-dependent mechanism and acquire an anti-tumor phenotype following cabozantinib treatment. These varied immunologic consequences of neutrophil infiltration within tumors are likely related to differences in mutational background and chemokine milieu within the tumor microenvironment.

HMGB1 has dual roles as a nuclear protein that regulates transcription and nucleosome assembly, and a “danger” signal that elicits immune responses when released into the extracellular space. In the latter context, HMGB1 can engage TLR2, TLR4, and receptor for advanced glycation end products (RAGE), in addition to CXCR4, resulting

in activation of innate immune effector functions. Moreover, Mac-1-dependent neutrophil recruitment to inflammatory sites induced by HMGB1 requires the presence of RAGE receptors on neutrophils (43). Because HMGB1 release occurs during immunogenic or necrotic cell death but not as a consequence of apoptotic cell death (44), the finding that HMGB1 release following cabozantinib treatment is required for subsequent tumor regression supports an immune-based anticancer mechanism for cabozantinib (Fig. 4E and F). In this context, HMGB1 likely activates both CXCR4 and CXCR4-independent mechanisms to elicit neutrophil-mediated antitumor innate immunity that is responsible for the observed tumor regression. Interestingly, we did not observe an increase in HMGB1 release following cabozantinib treatment of PTEN wild-type, p53-mutant human prostate cancer cells. These data suggest that PTEN wild-type prostate cancer cells may be less susceptible to immunogenic cell death than PTEN-deficient prostate cancer cells. However, due to the limited availability of prostate cancer cell lines, it is not possible to make a definitive statement about the effect of mutational background on cabozantinib-induced HMGB1 release.

The finding that cabozantinib provokes an innate immune response as part of its mechanism of action has profound implications for its use in the presence of treatment regimens that may compromise immune function, such as prior myeloablative chemotherapy or immune suppressive steroid use. Cabozantinib has received FDA approval in two different solid malignancies, MTC (6) and RCC (9, 10). Both MTC and RCC typically do not respond to chemotherapy, so the patients enrolled in these trials were typically chemo-naïve. On the other hand, patients in the CRPC phase III trial were pretreated with docetaxel chemotherapy, which may potentially explain the failure of the CRPC trial to meet its OS endpoint (8). In addition to neutrophil depletion, plerixafor treatment and HMGB1 neutralization, concomitant dexamethasone treatment also attenuated cabozantinib-mediated tumor clearance in our study (Supplementary Fig. S8). This observation is clinically significant because patients with advanced prostate cancer are often treated with concomitant steroids, which could interfere with antitumor immune responses elicited by hormonal and/or cytotoxic chemotherapy (45).

There has been considerable enthusiasm about T-cell checkpoint blockade-based therapies in patients with advanced cancer. In melanoma, RCC, and non-small cell lung cancer, adaptive T cell-based immune checkpoint blockade strategies (PD-1/PD-L1 inhibitors) have already received FDA approval. However, there are still subsets of patients across all malignancies that fail to respond to these therapies. In specific malignancy types, such as CRPC (46, 47) and pancreatic ductal adenocarcinoma (48), very few responses to these T-cell checkpoint blockade therapies have been reported, highlighting a strong unmet need for investigating combination therapies to improve clinical responses to CTLA-4 and/or PD-1/PD-L1 blockade. The combination of cabozantinib with approaches that activate adaptive immunity, such as T-cell checkpoint blockade or vaccine-based approaches, may provide durable benefit in patients with advanced cancer and warrant further investigation.

METHODS

Mice and In Vivo Drug Treatment

All studies were performed on protocols approved by Beth Israel Deaconess Medical Center Institutional Animal Care and Use Committees. Mouse strains with Probasin Cre-driven conditional prostate-specific knockout of *Pten* and *Trp53* genes (*Pb-Cre*; *Pten^{f/f}/Trp53^{f/f}*) have been previously described (14). Following breeding of *Pb-Cre*; *Pten^{f/f}/Trp53^{f/f}* males with *Pten^{f/f}/Trp53^{f/f}* females, all genotypes were confirmed by PCR. The experimental male *Pb-Cre*; *Pten^{f/f}/Trp53^{f/f}* mice underwent screening ultrasound beginning at 4 months of age, and then every 1 to 2 weeks until the development of a solid tumor > 5 mm in long axis diameter. The development of the solid tumor was confirmed by MRI, and then the mice were assigned to different treatment arms. The mice were treated with cabozantinib (Active-Biochem, 100 mg/kg in water) or PF-04217903 (c-MET inhibitor, Selleck, 50 mg/kg in methylcellulose) administered by once-daily oral gavage. At the end of the treatment period, anterior prostate tumor tissue was harvested and fixed in 4% paraformaldehyde or zinc-based fixative for histopathologic analysis, snap-frozen in liquid nitrogen for RNA profiling or dissociated in 2 mg/mL collagenase IV (Worthington Biochemical Corp.)/2 mg/mL DNase (Sigma) for flow cytometry analysis. For pretreatment studies, intraperitoneal injections were administered for the following drugs: dexamethasone (Sigma, 5 mg/kg daily in PBS), plerixafor (Sigma, 1 mg/kg daily injection or ALZET osmotic pump 1007D loaded with 90 mg/mL), Ly6G-depletion antibody (1A8, BioXcell, 200 µg daily diluted in PBS), and HMGB1-neutralizing antibody (3E8, BioLegend, 2.5 mg/kg every other day) were administered via intraperitoneal injection, during the pretreatment phase for 3 days, followed by 3 days of concomitant treatment with cabozantinib. For T-cell and NK-cell depletion studies, anti-CD4 depleting antibody (BioLegend 300 µg) and anti-CD8 antibody (BioLegend 300 µg) were administered as a single intaperitoneal injection daily during the pretreatment phase of 3 days (day -3 to day -1), followed by a single injection on day +2 with concomitant cabozantinib treatment (days 0-3). For NK-cell depletion, anti-sialo GM1 antibody (100 µg) was administered as a single injection 3 days prior to cabozantinib (day -3), and a repeat injection on day 0, concomitant with initiation of cabozantinib treatment (days 0-3).

Ultrasound Screening of Mice for Development of Solid Prostate Tumors

High-resolution ultrasound imaging of mouse prostate was carried out using the Vevo 2100 System (Visual Sonics, Inc.). Briefly, mice of 4 to 5 months of age were anesthetized with a 3% isoflurane/oxygen mixture. Abdominal hair was removed by shaving and depilatory cream was applied, followed by ample washing with sterile water to prevent irritation to the skin. Ultrasound gel was applied to the abdominal area of the mice and scanning performed with a 32- to 56-MHz Mircoscan transducer (MS-550S, Visual Sonics, Inc.).

PET/MRI Imaging and Volumetric Analysis of Mouse Prostate Tumors

All mice were anesthetized with a mixture of isoflurane and oxygen (2.5/2.0%) for 10 minutes prior to injection of ¹⁸F-FDG. Approximately 350 µCi (50 µL) of ¹⁸F-FDG was injected retro-orbitally. Sixty minutes after injection, mice were imaged by PET/CT using a NanoPET/CT (Mediso Medical Imaging Systems). Scout images were acquired, and the center of the field of view (FOV) for PET imaging was selected manually to be in the region of prostate/bladder. All mice were scanned for 30 minutes by PET. Following PET acquisition, mice were immediately transported from the PET scanner to an ASPECT Model M2 1T tabletop MRI scanner (ASPECT Magnet Technologies Ltd.). All mice

were placed in a 35-mm mouse radiofrequency (RF) coil, calibrated to a RF frequency of between 43 and 45 MHz, which is used for both transmission and reception. Anesthesia was maintained using isoflurane/oxygen anesthesia via an external vaporizer maintained at a percentage of 2.0% and 1.5%, and respiration was monitored using a small animal physiologic monitoring system (BIOPAC Systems, Inc.). Scout/localizer images were acquired using a GRE steady-state sequence to acquire images in all three orthogonal planes/orientations. For prostate MRI, mice were positioned in the center of the magnet with bladder used as the anatomical reference for the center point (similar to PET acquisition). Axial T2-weighted SE images were acquired with the following parameters: FOV 40 × 40 mm, 1/0 mm thickness/gap, TR/TE of 4,600/40 ms, 256 × 256 matrix, 2 NEX, and a dwell time of 30 µs. The NRG Console GUI (ASPECT) was utilized for online reconstruction, which enables data to be converted into DICOM files and archived for export into Vivoquant (inVICRO Inc.) image analysis software. PET and MRI DICOM files were loaded into the same window and manually adjusted for coregistration. Anatomical landmarks, i.e., bladder and heart, were used to register images. Volumetric analysis was performed using PACS software, which was developed at Beth Israel Deaconess Medical Center (BIDMC).

Hematoxylin and Eosin Staining and IHC

For anti-pMET antibody (pYpYpY1230/1234/1235 Invitrogen Cat # 44888G), tissues were fixed in 4% paraformaldehyde (PFA) and embedded in paraffin according to standard procedures. For all other antibodies utilized in this study, <3-mm-thick prostate tumor tissues were fixed in Tris-based zinc fixative (BD Pharmingen) for 36 hours at room temperature, dehydrated in a propanolol-based tissue processor, and embedded in paraffin for sectioning. Approximately 5-µm-thick sections were baked for 10 minutes, deparaffinized, rehydrated, and post-fixed with cold acetone:formalin 95:5 (vol/vol) for 3 minutes. The sections were then incubated with horse serum (7% in PBS) prior to overnight incubation at 4°C with the following antibodies: Ly6G (LifeSpan BioSciences Inc.), myeloperoxidase (Thermo Fisher Scientific), ICAM1 (BD Pharmingen), CD86 (BioLegend), cleaved caspase-3 (Cell Signaling Technology 9664), and granzyme B (Abcam). Sections were then treated with H₂O₂ 1:100 in PBS for 10 minutes, incubated with the appropriate secondary IgG antibodies followed by ABC (avidin-biotin complex) reagent (Vector Laboratories), then detected by ImmPACT 3,3'-diaminobenzidine tetrahydrochloride (DAB) peroxidase substrate (Vector Laboratories).

For PTEN IHC, deparaffinization and epitope retrieval was performed by EnVision FLEX, pH 9.0 (Link-K8000; Dako North America, Inc.). Immunostaining was performed using a DAKO autostainer (Autostainer Link 48; Dako North America, Inc.) following supplied protocol, using rabbit anti-PTEN monoclonal antibody (clone D4.3, Cell Signaling Technologies) at 1:100 dilution, and the reaction was visualized by DAB.

For quantitation of Ly6G and cleaved caspase-3 IHC staining, slides were digitized using a ScanScope XT (Leica Biosystems Inc.) and annotated using the program Aperio ImageScope (Version 12; Leica Biosystems Inc.). Afterward, an optimized nuclear algorithm was applied for Ly6G and caspase-3 analyses to identify cells positive for each stain across the entire tumor section on the slide.

Flow-Cytometry Analysis

After dissection, tumors were diced with razor blades and then digested by incubating at 37°C for 1 hour in RPMI containing 10% fetal calf serum, 2 mg/mL Collagenase IV, and 2 mg/mL DNase I. Splenocytes were obtained by macerating spleens through 70-µm nylon mesh; red blood cells were lysed by hypotonic lysis using 0.2% NaCl equilibrated to 0.9% NaCl after 30 seconds incubation at room temperature. Single-cell suspensions for both tumor and spleen

samples were obtained by straining through a 70-μm mesh filter, and cells were washed twice in FACS buffer (PBS containing 0.5% bovine serum albumin and 0.01% sodium azide). Cells were stained with indicated fluorophore conjugated antibodies (BioLegend) and analyzed using a Gallios Flow Cytometer (Beckman Coulter).

For HMGB1 cellular depletion assay, cells were recovered using trypsin/EDTA, fixed in 4% PFA in PBS, permeabilized in ice-cold methanol and incubated for at least 30 minutes in -20°C. Cells were then rehydrated in PBS, washed in FACS buffer, and incubated for 1 hour in anti-HMGB1 (MBL International Corp.), washed and then incubated for 30 minutes with anti-mouse IgG conjugated with Alexa488 (Life Technologies) and subjected to flow cytometry analysis using a BD FACS Calibur.

Targeted Mass Spectrometry (LC/MS) for Intratumoral Cabozantinib Quantification

Tissue samples were disrupted in 500 μL 80% methanol using the TissueLyser II and stainless steel beads at 28 Hz for 90 seconds for 3 rounds, according to protocol as previously described (49). The tissue was pelleted at 14,000 rpm for 5 minutes at 4°C. The supernatant was collected, and the volume equivalent to 10 ng was desiccated in a Speed Vac. Throughout processing, the samples were chilled in a dry ice/ethanol bath. A 10 μL sample was injected and analyzed using a 5500 QTRAP hybrid triple quadrupole mass spectrometer (AB/SCIEX). The 5500 QTRAP hybrid triple quadrupole mass spectrometer (AB/SCIEX) was coupled to a Prominence UFC HPLC system (Shimadzu) via selected reaction monitoring (SRM) for the Q1/Q3 transition of 500.2/295.2 for cabozantinib. ESI voltage was +4900V in positive ion mode using a dwell time of 4 ms and collision energy of 45. Approximately 15 data points were obtained for cabozantinib per LC/MS-MS experiment. Samples were delivered to the MS via hydrophilic interaction chromatography (HILIC) using a 4.6 mm i.d. × 10 cm Amide Xbridge column (Waters) at 350 μL/minute and cabozantinib eluted at ~3.45 minutes. Gradients were run starting from 85% buffer B (HPLC grade acetonitrile) to 42% B from 0 to 5 minutes; 42% B to 0% B from 5 to 16 minutes; 0% B was held from 16 to 24 minutes; 0% B to 85% B from 24 to 25 minutes; 85% B was held for 7 minutes to reequilibrate the column. Cabozantinib was eluted at approximately 3.50 minutes. Buffer A was comprised of 20 mmol/L ammonium hydroxide/20 mmol/L ammonium acetate (pH = 9.0) in 95:5 water:acetonitrile. Peak areas from the total ion current for the cabozantinib metabolite SRM transition were integrated using MultiQuant v2.0 software (AB/SCIEX). For the concentration curve data, cabozantinib was prepared at concentrations of 1 nmol/L, 250 nmol/L, 500 nmol/L, 1 μmol/L, 10 μmol/L, and 30 μmol/L in 40% methanol. Five microliters of each sample was injected using the parameters described above.

Cell Culture and Apoptosis Assays

PC3, VCAP, 22Rv1, and DU145 prostate cancer cells were purchased from the ATCC in February 2016, where they had been authenticated by short tandem repeat profiling. PC3, VCAP, and DU145 cells were cultured in Dulbecco's Modified Eagle Medium (DMEM) supplemented with 10% FBS. 22Rv1 cells were cultured in Roswell Park Memorial Institute (RPMI) media supplemented with 10% FBS. AC1, AC3, and SC1 cells (all derived from murine PTEN/p53-deficient prostate tumors) were obtained from and authenticated by the Kelly laboratory in July 2013, at the NCI (50). AC1 cells were cultured in PrEGM BulletKit media (Lonza Inc.). AC3 and SC1 cells were cultured in PrEGM BulletKit media supplemented with 10% FBS. All cell lines were routinely tested for *Mycoplasma* (MycoAlert; Lonza).

For cell death assays, the cells were treated with 10 or 30 μmol/L cabozantinib. Apoptosis was performed using Annexin V:FITC Apoptosis Detection Kit I. Apoptosis data were analyzed using BD LSR II Flow Cytometer and FlowJo software. For HMGB1 depletion

and assays, cells were treated with cabozantinib (10 or 30 μmol/L), doxorubicin (1 μmol/L), or DMSO control, and analyzed by flow cytometry.

RNA Sequencing and Gene Set Enrichment Analysis

RNA sequencing on murine *Pten*^{fl/fl}*Trp53*^{fl/fl} whole tumors was performed using standard protocols involving RNA integrity check, poly-A selection, and TruSeq library preparation. Gene set enrichment analysis was performed using application default parameters and MSigDB gene sets. Sequencing was performed on the Illumina HiSeq2500 with 5 to 6 samples per lane. Short reads (PE 2 × 75) were aligned to the mm9 reference genome using TopHat with default parameters. Cufflinks with GC and upper quartile normalization was used to calculate gene expression levels for all RefSeq genes (annotation downloaded from UCSC on March 2014). Quality control was performed using FastQC and visual analysis using R and IGV. For heat map visualization, genes expression levels were normalized to a 0–1 scale using maximum expression across all samples analyzed and represented using a green–black–red color scale.

Real-time Quantitative PCR

For gene expression analysis from murine PTEN/p53-deficient whole tumors, RNA was isolated using an RNEasy isolation kit (Qiagen) according to the manufacturer's protocol. Reverse transcription was conducted on 1 μg of total RNA using iScript cDNA Synthesis Kit (BioRad). Real-time quantitative PCR (RT-qPCR) analyses was performed using QuantiFast SYBR Green PCR Kit (Qiagen). A comparative CT (threshold cycle) was used to determine gene expression and analyzed against the endogenous genes of murine β-actin. The experiments were carried out three times in triplicate (3 to 4 mice per group). Specific primers for the following genes were obtained from Integrated DNA Technologies: murine CXCL12: 5' TGCATCAGT GACGGTAAACCA 3', 5' TTCTTCAGCCGTGACAATC 3'; murine CXCR4: 5' GAAGTGGGGCTGGAGACTAT 3', 5' TTGCCGACTAT GCCAGTCAG 3'; murine CD86: 5' forward – TCA ATG GGA CTG CAT ATC TGC C 3', reverse – 5' CAG CTC ACT CAG GCT TAT GTT TT 3'; murine CD3: 5' AGCGGGATTCTGGCTAGTCT 3', 5' CGCTG GTATTGCAAGTCACAA 3'; murine CD4: 5' TCCTAGCTGCACT CAAGGGA 3', 5' TCAGAGAACCTCCAGGTGAAGA 3'; murine CD8: 5' CCGTTGACCCGTTCTGT 3', 5' CGCGTCCATTCTTTG GAA 3'; and murine NKG2D: 5' ACTCAGAGATGAGCAAATGCC 3', 5' CAGGTTGACTGGTAGTTAGTGC 3'.

ELISA and Phospho-RTK Proteomic Assays

For ELISA analysis, SC1, VCaP, 22Rv1, and DU145 cells were treated with DMSO, cabozantinib (10 μmol/L), or doxorubicin (1 μmol/L) for 32 hours. ELISA was performed for CXCL12 (R&D Systems) and/or HMGB1 (LSBio Inc.) on cell culture supernatant as indicated, according to the manufacturer-supplied protocols. For phospho-RTK proteomic analysis (R&D Systems), human and murine prostate cancer cell lines were treated with DMSO or cabozantinib (10 μmol/L) for indicated times, and then cell lysates were analyzed according to the manufacturer supplied protocol.

RNA In Situ Hybridization

Formalin-fixed, paraffin-embedded (FFPE) tissues were cut into 4-μm-thick serial sections. RISH was performed using mouse CXCL12 probe (Advanced Cell Diagnostics) and RNAscope detection kit 2.0 HD Red (Advanced Cell Diagnostics) according to the manufacturer-supplied protocol.

Combined In Situ Hybridization and IHC

In situ hybridization for CXCL12 was performed using mouse CXCL12 probe as described above. After the signal detection step,

slides were rinsed in distilled water, stained with anti-PTEN antibody at 1:100 using a DAKO autostainer following supplied protocol, and the reaction was visualized by DAB.

Human Neutrophil Isolation and Ex Vivo Neutrophil Migration Assay

All neutrophils were isolated from 10 mL of whole human blood with EDTA as an anticoagulant (Research Blood Components) by negative selection using the EasySep human neutrophil isolation kit (StemCell Technologies Cat #19666). PC3 cells (ATCC) were cultured in RPMI-1640 (Life Technologies) supplemented with 10% FBS (Life Technologies) and 10% PenStrep (Life Technologies). PC3 cells were then plated on 24-well plates (Greiner Bio One, Cat. #89131-690) at a density of 60,000 cells/well. A working volume of 500 μL of media was used throughout the experiments. After plating, cells were allowed to adhere for 24 hours. Following attachment, PC3 cells were treated with 5 μmol/L cabozantinib or DMSO (vehicle control) in unsupplemented serum-free RPMI-1640 for 24 hours. Freshly isolated human neutrophils (200,000) were then placed in the top of the 3-μm polycarbonate Transwell insert (Corning, Cat. # 29442-110) in 100 μL of unsupplemented serum-free RPMI-1640. Cells were incubated at 37°C for 4 hours. Media (100 μL) was then collected from the bottom of the Transwell. A 30 μL sample was then analyzed using flow cytometry to count the number of migrated neutrophils. For blocking experiments, anti-HMGB1 clone 3E8 was added to cabozantinib-treated PC3 cells to a final concentration of 50 μg/mL and incubated for 1 hours at 37°C.

Nitric Oxide Staining

PC3 cells were cultured as described above, and then plated on 96-well plates (Greiner Bio One, Cat. # 655180) at a density of 20,000 cells per well and allowed to adhere for 24 hours following plating. Cells were then treated with 5 μmol/L cabozantinib or DMSO (vehicle control) in RPMI-1640 supplemented with 0.5% BSA for 24 hours.

Freshly isolated human neutrophils were then cocultured with PC3 cells treated with DMSO (vehicle-treated) in basal RPMI, and PC3 cells treated with 5 μmol/L cabozantinib for 6 hours. In parallel, neutrophils were also cultured in media alone and media containing 5 μmol/L cabozantinib for 6 hours to assess the impact of cabozantinib on activation of neutrophils.

Approximately 500,000 neutrophils were cocultured for a 1:25 PC3:neutrophil ratio. After 6 hours, cell culture supernatant containing neutrophils was collected and centrifuged at 1,800 rpm for 5 minutes. Cells were resuspended in 20 mmol/L HEPES buffer solution in PBS and stained with DAF-FM diacetate in DMSO (Molecular Probes, Cat. # D-23844) at a final concentration of 5 μmol/L. Cells were stained for 15 minutes at 37°C as described previously (51). Cells were washed once in 20 mmol/L HEPES in PBS, and analysis was performed immediately by flow cytometry.

Statistical Analysis

GraphPad Prism 6 software (GraphPad Software Inc.) was used for all statistical analyses. The results are presented as mean ± standard deviation. Paired *t* tests were used to assess the statistical significance of the change in gene/chemokine protein levels at baseline and following cabozantinib treatment. Values of *P* < 0.05 were considered statistically significant. For statistical analysis of the Ly6G and caspase-3 IHC data, a one-way analysis of variance (ANOVA) followed by a Tukey *post hoc* test was performed with a *P* < 0.05 level of significance. For neutrophil migration experiments (including HMGB1 blocking by Anti-HMGB1), a one-way ANOVA test, using Sidak's multiple comparison method, was performed with a *P* < 0.05 level of significance. For analyzing the increase in nitric oxide production, a one-way ANOVA test followed by a Tukey *post hoc* test was performed with a *P* < 0.05 level of significance.

Disclosure of Potential Conflicts of Interest

No potential conflicts of interest were disclosed.

One of the Editors-in-Chief is an author on this article. In keeping with the AACR's editorial policy, the peer review of this submission was managed by a senior member of *Cancer Discovery*'s editorial team; a member of the AACR Publications Committee rendered the final decision concerning acceptability.

Authors' Contributions

Conception and design: A. Patnaik, K.D. Swanson, L.C. Cantley

Development of methodology: A. Patnaik, K.D. Swanson, A. Solanki, M.P. Gehring, A.R. Pyzer, L. Montaser, H. Ye

Acquisition of data (provided animals, acquired and managed patients, provided facilities, etc.): A. Patnaik, K.D. Swanson, A. Solanki, N. Landon-Brace, M.P. Gehring, K. Helenius, B.M. Olson, A.R. Pyzer, L.C. Wang, J. Novak, J.M. Asara, J.J. Timmons, T.M. Morgan, Y. Wang, E. Levantini, J.G. Clohessy, K. Kelly, P.P. Pandolfi, J.M. Rosenblatt, H. Ye, S. Signoretti

Analysis and interpretation of data (e.g., statistical analysis, biostatistics, computational analysis): A. Patnaik, K.D. Swanson, A. Solanki, N. Landon-Brace, M.P. Gehring, K. Helenius, A.R. Pyzer, L.C. Wang, O. Elemento, J. Novak, T.B. Thornley, J.M. Asara, J.J. Timmons, T.M. Morgan, Y. Wang, E. Levantini, D.E. Avigan, H. Ye, J.M. Karp, S. Signoretti, S.P. Balk

Writing, review, and/or revision of the manuscript: A. Patnaik, K.D. Swanson, A. Solanki, N. Landon-Brace, K. Helenius, J. Novak, J.M. Asara, T.M. Morgan, J.M. Rosenblatt, H. Ye, J.M. Karp, S. Signoretti, S.P. Balk, L.C. Cantley

Administrative, technical, or material support (i.e., reporting or organizing data, constructing databases): A. Patnaik, J. Novak, Y. Wang, L.C. Cantley

Study supervision: A. Patnaik, D.E. Avigan, J.M. Karp, L.C. Cantley

Other (histology and immunohistochemistry data): E. Csizmadia

Acknowledgments

We thank the Small Animal Imaging Core at BIDMC for the FDG-PET/MRI studies to support relevant mouse experiments. We also thank Dr. Philip Sharp from the Koch Institute at MIT for providing resources for RNA analysis in his laboratory. We thank Kimberly McClinch and Durga Kolla for providing editorial assistance with the manuscript.

Grant Support

This work was partially supported by the following funding sources: Prostate P01 P01CA089021 (L.C. Cantley), R01 GM041890 (L.C. Cantley), Dana Farber/Harvard Cancer Center SPORE Career Development Award 5 P50 CA090381-08 (A. Patnaik), Prostate Cancer Foundation Young Investigator Award (A. Patnaik), and Department of Defense Physician Researcher Training Award-W81XWH-11-1-0298 (A. Patnaik). K.D. Swanson was partially supported by Reason to Ride Cancer Charity Fund.

Received July 15, 2016; revised October 7, 2016; accepted March 6, 2017; published OnlineFirst March 8, 2017.

REFERENCES

1. Coussens LM, Werb Z. Inflammation and cancer. *Nature* 2002;420:860–7.
2. Dunn GP, Bruce AT, Ikeda H, Old LJ, Schreiber RD. Cancer immunoediting: from immunosurveillance to tumor escape. *Nat Immunol* 2002;3:991–8.
3. Condeelis J, Pollard JW. Macrophages: obligate partners for tumor cell migration, invasion, and metastasis. *Cell* 2006;124:263–6.
4. Jessy T. Immunity over inability: The spontaneous regression of cancer. *J Natl Sci Biol Med* 2011;2:43–9.

5. Yakes FM, Chen J, Tan J, Yamaguchi K, Shi Y, Yu P, et al. Cabozantinib (XL184), a novel MET and VEGFR2 inhibitor, simultaneously suppresses metastasis, angiogenesis, and tumor growth. *Mol Cancer Ther* 2011;10:2298–308.
6. Nix NM, Braun K. Cabozantinib for the treatment of metastatic medullary thyroid carcinoma. *J Adv Pract Oncol* 2014;5:47–50.
7. Smith DC, Smith MR, Sweeney C, Elfiky AA, Logothetis C, Corn PG, et al. Cabozantinib in patients with advanced prostate cancer: results of a phase II randomized discontinuation trial. *J Clin Oncol* 2013;31:412–9.
8. Smith M, De Bono J, Sternberg C, Le Moulec S, Oudard S, De Giorgi U, et al. Phase III study of cabozantinib in previously treated metastatic castration-resistant prostate cancer: COMET-1. *J Clin Oncol* 2016;34:3005–13.
9. Choueiri TK, Escudier B, Powles T, Tannir NM, Mainwaring PN, Rini BI, et al. Cabozantinib versus everolimus in advanced renal cell carcinoma (METEOR): final results from a randomised, open-label, phase 3 trial. *Lancet Oncol* 2016;17:917–27.
10. Choueiri TK, Escudier B, Powles T, Mainwaring PN, Rini BI, Donskov F, et al. Cabozantinib versus everolimus in advanced renal-cell carcinoma. *N Engl J Med* 2015;373:1814–23.
11. Robinson D, Van Allen EM, Wu YM, Schultz N, Lonigro RJ, Mosquera JM, et al. Integrative clinical genomics of advanced prostate cancer. *Cell* 2015;161:1215–28.
12. Grasso CS, Wu YM, Robinson DR, Cao X, Dhanasekaran SM, Khan AP, et al. The mutational landscape of lethal castration-resistant prostate cancer. *Nature* 2012;487:239–43.
13. Lunardi A, Ala U, Epping MT, Salmena L, Clohessy JG, Webster KA, et al. A co-clinical approach identifies mechanisms and potential therapies for androgen deprivation resistance in prostate cancer. *Nat Genet* 2013;45:747–55.
14. Chen Z, Trotman LC, Shaffer D, Lin HK, Dotan ZA, Niki M, et al. Crucial role of p53-dependent cellular senescence in suppression of Pten-deficient tumorigenesis. *Nature* 2005;436:725–30.
15. Wanjala J, Taylor BS, Chapinski C, Hieronymus H, Wongvipat J, Chen Y, et al. Identifying actionable targets through integrative analyses of GEM model and human prostate cancer genomic profiling. *Mol Cancer Ther* 2015;14:278–88.
16. Kurzrock R, Sherman SI, Ball DW, Forastiere AA, Cohen RB, Mehra R, et al. Activity of XL184 (Cabozantinib), an oral tyrosine kinase inhibitor, in patients with medullary thyroid cancer. *J Clin Oncol* 2011;29:2660–6.
17. Furusato B, Mohamed A, Uhlen M, Rhim JS. CXCR4 and cancer. *Pathol Int* 2010;60:497–505.
18. Christopher MJ, Link DC. Regulation of neutrophil homeostasis. *Curr Opin Hematol* 2007;14:3–8.
19. Schiraldi M, Raucci A, Munoz LM, Livoti E, Celona B, Venereau E, et al. HMGB1 promotes recruitment of inflammatory cells to damaged tissues by forming a complex with CXCL12 and signaling via CXCR4. *J Exp Med* 2012;209:551–63.
20. Ding HS, Yang J, Gong FL, Yang J, Ding JW, Li S, et al. High mobility group [corrected] box 1 mediates neutrophil recruitment in myocardial ischemia-reperfusion injury through toll like receptor 4-related pathway. *Gene* 2012;509:149–53.
21. Pietras K, Ostman A. Hallmarks of cancer: interactions with the tumor stroma. *Exp Cell Res* 2010;316:1324–31.
22. Friedman WH, Dieu-Nosjean MC, Pages F, Cremer I, Damotte D, Sautes-Fridman C, et al. The immune microenvironment of human tumors: general significance and clinical impact. *Cancer Microenviron* 2013;6:117–22.
23. Savill J, Gregory C. Apoptotic PS to phagocyte TIM-4: eat me. *Immunity* 2007;27:830–2.
24. Palombo F, Focaccetti C, Barnaba V. Therapeutic implications of immunogenic cell death in human cancer. *Front Immunol* 2014;4:503.
25. Fridlender ZG, Sun J, Kim S, Kapoor V, Cheng G, Ling L, et al. Polarization of tumor-associated neutrophil phenotype by TGF-beta: “N1” versus “N2” TAN. *Cancer Cell* 2009;16:183–94.
26. Mantovani A. The yin-yang of tumor-associated neutrophils. *Cancer Cell* 2009;16:173–4.
27. Piccard H, Muschel RJ, Opdenakker G. On the dual roles and polarized phenotypes of neutrophils in tumor development and progression. *Crit Rev Oncol Hematol* 2012;82:296–309.
28. Sionov RV, Fridlender ZG, Granot Z. The multifaceted roles neutrophils play in the tumor microenvironment. *Cancer Microenviron* 2015;8:125–58.
29. Mishalian I, Bayuh R, Levy L, Zolotarov L, Michaeli J, Fridlender ZG. Tumor-associated neutrophils (TAN) develop pro-tumorigenic properties during tumor progression. *Cancer Immunol Immunother* 2013;62:1745–56.
30. Zentay Z, Sharaf M, Qadir M, Drafta D, Davidson D. Mechanism for dexamethasone inhibition of neutrophil migration upon exposure to lipopolysaccharide in vitro: role of neutrophil interleukin-8 release. *Pediatr Res* 1999;46:406–10.
31. Rahman MM, Alkhouri H, Tang F, Che W, Ge Q, Ammit AJ. Sphingosine 1-phosphate induces neutrophil chemoattractant IL-8: repression by steroids. *PLoS One* 2014;9:e92466.
32. Massena S, Christoffersson G, Vagesjo E, Seignez C, Gustafsson K, Binet F, et al. Identification and characterization of VEGF-A-responsive neutrophils expressing CD49d, VEGFR1, and CXCR4 in mice and humans. *Blood* 2015;126:2016–26.
33. Yamada M, Kubo H, Kobayashi S, Ishizawa K, He M, Suzuki T, et al. The increase in surface CXCR4 expression on lung extravascular neutrophils and its effects on neutrophils during endotoxin-induced lung injury. *Cell Mol Immunol* 2011;8:305–14.
34. Zhou H, Wang Y, Wang W, Jia J, Li Y, Wang Q, et al. Generation of monoclonal antibodies against highly conserved antigens. *PLoS One* 2009;4:e6087.
35. Ilieva KM, Correa I, Josephs DH, Karagiannis P, Egbuniwe IU, Cafferkey MJ, et al. Effects of BRAF mutations and BRAF inhibition on immune responses to melanoma. *Mol Cancer Ther* 2014;13:2769–83.
36. Steinberg SM, Zhang P, Malik BT, Boni A, Shabaneh TB, Byrne KT, et al. BRAF inhibition alleviates immune suppression in murine autochthonous melanoma. *Cancer Immunol Res* 2014;2:1044–50.
37. Sottile R, Pangigadde PN, Tan T, Anichini A, Sabbatino F, Trecroci F, et al. HLA class I downregulation is associated with enhanced NK-cell killing of melanoma cells with acquired drug resistance to BRAF inhibitors. *Eur J Immunol* 2016;46:409–19.
38. Vella LJ, Pasam A, Dimopoulos N, Andrews M, Knights A, Puaux AL, et al. MEK inhibition, alone or in combination with BRAF inhibition, affects multiple functions of isolated normal human lymphocytes and dendritic cells. *Cancer Immunol Res* 2014;2:351–60.
39. Manzini C, Vene R, Cossu I, Guasco M, Zupo S, Dono M, et al. Cytokines can counteract the inhibitory effect of MEK-i on NK-cell function. *Oncotarget* 2016;7:60858–71.
40. Hu-Liesková S, Mok S, Homé Moreno B, Tsoi J, Robert L, Goedert L, et al. Improved antitumor activity of immunotherapy with BRAF and MEK inhibitors in BRAF(V600E) melanoma. *Sci Transl Med* 2015;7:279ra41.
41. Di Mitri D, Toso A, Chen JJ, Sarti M, Pinton S, Jost TR, et al. Tumour-infiltrating Gr-1+ myeloid cells antagonize senescence in cancer. *Nature* 2014;515:134–7.
42. Spiegel A, Brooks MW, Houshyar S, Reinhardt F, Ardolino M, Fessler E, et al. Neutrophils suppress intraluminal NK cell-mediated tumor cell clearance and enhance extravasation of disseminated carcinoma cells. *Cancer Discov* 2016;6:630–49.
43. Orlova VV, Choi EY, Xie C, Chavakis E, Bierhaus A, Ihanus E, et al. A novel pathway of HMGB1-mediated inflammatory cell recruitment that requires Mac-1-integrin. *EMBO J* 2007;26:1129–39.
44. Lotze MT, Tracey KJ. High-mobility group box 1 protein (HMGB1): nuclear weapon in the immune arsenal. *Nat Rev Immunol* 2005;5:331–42.
45. Wong ET, Lok E, Gautam S, Swanson KD. Dexamethasone exerts profound immunologic interference on treatment efficacy for recurrent glioblastoma. *Br J Cancer* 2015;113:232–41.

46. Schweizer MT, Drake CG. Immunotherapy for prostate cancer: recent developments and future challenges. *Cancer Metastasis Rev* 2014;33: 641–55.
47. Graff JN, Alumkal JJ, Drake CG, Thomas GV, Redmond WL, Farhad M, et al. Early evidence of anti-PD-1 activity in enzalutamide-resistant prostate cancer. *Oncotarget* 2016;7:52810–7.
48. Quinn BA, Lee NA, Kegelman TP, Bhoopathi P, Emdad L, Das SK, et al. The quest for an effective treatment for an intractable cancer: established and novel therapies for pancreatic adenocarcinoma. *Adv Cancer Res* 2015;127:283–306.
49. Yuan M, Breitkopf SB, Yang X, Asara JM. A positive/negative ion-switching, targeted mass spectrometry-based metabolomics platform for bodily fluids, cells, and fresh and fixed tissue. *Nat Protoc* 2012;7:872–81.
50. Martin P, Liu YN, Pierce R, Abou-Kheir W, Casey O, Seng V, et al. Prostate epithelial Pten/TP53 loss leads to transformation of multi-potential progenitors and epithelial to mesenchymal transition. *Am J Pathol* 2011;179:422–35.
51. Finisguerra V, Di Conza G, Di Matteo M, Serneels J, Costa S, Thompson AA, et al. MET is required for the recruitment of anti-tumoural neutrophils. *Nature* 2015;522:349–53.

CANCER DISCOVERY

Cabozantinib Eradicates Advanced Murine Prostate Cancer by Activating Antitumor Innate Immunity

Akash Patnaik, Kenneth D. Swanson, Eva Csizmadia, et al.

Cancer Discov 2017;7:750-765. Published OnlineFirst March 8, 2017.

Updated version

Access the most recent version of this article at:
doi:[10.1158/2159-8290.CD-16-0778](https://doi.org/10.1158/2159-8290.CD-16-0778)

Supplementary Material

Access the most recent supplemental material at:
<http://cancerdiscovery.aacrjournals.org/content/suppl/2017/03/08/2159-8290.CD-16-0778.DC1>

Cited articles

This article cites 51 articles, 13 of which you can access for free at:
<http://cancerdiscovery.aacrjournals.org/content/7/7/750.full#ref-list-1>

E-mail alerts

[Sign up to receive free email-alerts](#) related to this article or journal.

Reprints and Subscriptions

To order reprints of this article or to subscribe to the journal, contact the AACR Publications Department at pubs@aacr.org.

Permissions

To request permission to re-use all or part of this article, contact the AACR Publications Department at permissions@aacr.org.